ACS APPLIED MATERIALS & INTERFACES

Research Article

www.acsami.org

Nanoparticle Cluster Gas Sensor: Controlled Clustering of SnO_2 Nanoparticles for Highly Sensitive Toluene Detection

Koichi Suematsu,*[,†] Yuka Shin,[‡] Zhongqiu Hua,[‡] Kohei Yoshida,[‡] Masayoshi Yuasa,[†] Tetsuya Kida,[†] and Kengo Shimanoe[†]

[†]Department of Energy and Material Sciences, Faculty of Engineering Science, Kyushu University, Kasuga, Fukuoka 816-8580, Japan

[‡]Department of Molecular and Material Science, Interdisciplinary Graduate School of Engineering Science, Kyushu University, Kasuga, Fukuoka, 816-8580, Japan

ABSTRACT: Gas sensing with nanosized oxide materials is attracting much attention because of its promising capability of detecting various toxic gases at very low concentrations. In this study, using clustered SnO_2 nanoparticles formed by controlled particle aggregation, we fabricated highly sensitive gas sensing films to detect large gas molecules such as toluene. A hydrothermal method using stanic acid ($SnO_2 \cdot nH_2O$) gel as a precursor produced monodispersed SnO_2 nanoparticles of ca. 5 nm at pH 10.6. Decreasing the solution pH to 9.3 formed SnO_2 clusters of ca. 45 nm that were assemblies of the monodispersed nanoparticles, as determined by dynamic light scattering, X-ray diffraction, and transmission electron microscopy analyses. Porous gas sensing films were successfully fabricated by a spin-coating method using the clustered nanoparticles due to the loose packing of the larger aggregated particles. The sensor devices using the porous films showed improved sensor responses (sensitivities) to H_2 and CO at 300 °C. The enhanced sensitivity resulted from an increase in the film's porosity, which promoted the gas diffusivity of the sensing films. Pd loading onto the clustered nanoparticles further upgraded the sensor response due to catalytic and electrical sensitization effects of Pd. In particular, the Pd-loaded SnO_2 nanoparticle clusters showed excellent sensitivity to toluene, able to detect it at down to low ppb levels.

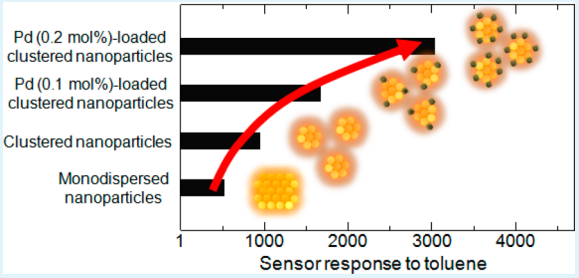

KEYWORDS: *SnO_2, cluster nanoparticles, Pd loading, hydrothermal method, gas diffusion, toluene*

INTRODUCTION

Controlling the size and shape of semiconductor materials is crucial to make good use of their functionality. SnO_2 is one of the multifunctional materials having a variety of applications such as gas sensors,[1−4] catalysis,[5,6] optoelectronic devices,[7−9] transparent conducting electrodes,[10,11] and electrodes for Li-ion batteries.[12−14] The good stability,[15] nontoxicity, and low cost of SnO_2 allow for its reliable commercial applications.[16] The most widely used application is as a gas sensor because of its high sensitivity to combustible gases. This application relies on the reaction of oxygen adsorbed on the SnO_2 surface with combustible gases such as hydrogen and carbon monoxide. The combustion reaction generates a change in the electrical resistance by releasing electrons trapped by adsorbed oxygen back to the SnO_2 surface. The resulting change in the electric resistance is used as a "sensor response" to know the presence and concentration of combustible gases in atmospheres.

Particularly, for gas sensor applications, the crystallite size control of SnO_2 is known to greatly improve its device performance. Xu et al. reported that decreasing the crystallite size of SnO_2 in the nanosize regime increased the sensor response to hydrogen and carbon monoxide.[17] This phenomenon can be explained in terms of spreading of the electron depletion region in the whole nanosized crystals by oxygen adsorption. The crystal size effect on the sensor response has recently been remodeled by Yamazoe et al.,[18,19] who postulated a new type of electron depletion designated "volume depletion", which occurs upon decreasing the crystallite size and donor density as well as increasing the oxygen partial pressure. When combustible gases react with the adsorbed oxygen, a highly electron depleted state disappears, generating a large change in the electrical resistance, i.e., large sensor response. Thus, decreasing the crystallite size of SnO_2 is one of the efficient ways to obtain high sensitivity (sensor response).

Another way to improve the sensor response is surface modification. Generally, loading metals or metal oxides such as Pd/PdO, and Pt on the SnO_2 surface increases the sensor response to combustible gases[20,21] and the gas selectivity.[21,22] Koziej et al. theoretically considered that Pd on the SnO_2 surface provides reaction sites for oxygen adsorption and combustion (chemical sensitization).[23] This is because the surface Pd can lower the energy barriers of the gas adsorption and gas dissociation, which catalytically facilitates combustion reactions. Electrical sensitization effects of Pd/PdO have also been revealed.[24] On the other hand, Hübnar et al. showed that Au clusters that were loaded on SnO_2 particles improved the

Received: February 13, 2014
Accepted: March 17, 2014
Published: March 17, 2014

   dx.doi.org/10.1021/am500944a | ACS Appl. Mater. Interfaces 2014, 6, 5319−5326

Scheme 1. Fabrication of Porous Gas Sensing Films Using Clustered SnO_2 Nanoparticles[a]

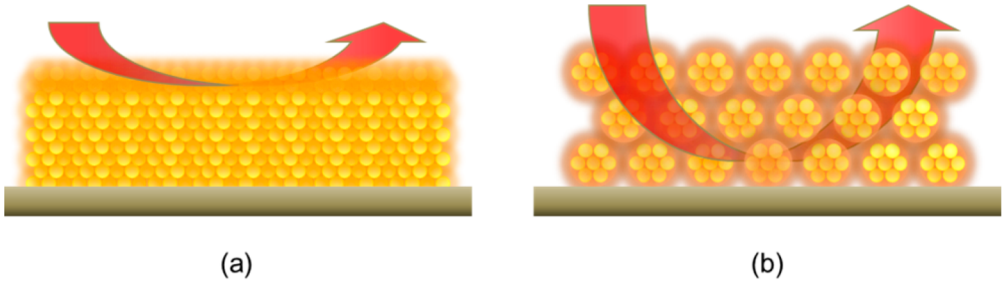

[a](a) and (b) represent gas diffusion in films made with monodispersed nanoparticles and clustered nanoparticles, respectively.

gas response.[25] They suggested that the response enhancement is caused by chemical sensitization effects resulting from gas spillover on metal clusters and by electrical sensitization effects resulting from Fermi level changes near the metal/semiconductor interfaces.

We also revealed the significant importance of pore size control of sensing films to detect large molecular gases. In particulate sensing films, target gases diffuse through pores that are formed by particle assembly. Gas diffusion depth is one of the important factors that remarkably affect the sensor response because insufficient diffusion inside the sensing films induces little change in electrical resistance of the films. Sakai et al. simulated the diffusion dependent sensor response to combustible gases according to gas concentration profiles inside sensing films:[26]

$$S = \frac{R_a}{R_g} = 1 + \frac{aC_{A,S}}{m}\tanh m, \quad m = L\sqrt{\frac{k}{D_K}} \tag{1}$$

where S is the sensor response, R_a and R_g are the electric resistance in synthetic air and combustible gas respectively, a is constant defined as sensitivity coefficient, $C_{A,S}$ is gas concentration at the surface, L is the thickness of a sensing film, k is the rate constant of surface reaction (reaction of adsorbed oxygen with combustible gases) and D_K is the Knudsen diffusion coefficient. Sensing films made with nanosized particles usually have pore radius ranging from 1 to 100 nm. Thus, Knudsen diffusion prevails in such films. The diffusion coefficient can be expressed by the following equation:

$$D_K = \frac{4r}{3}\sqrt{\frac{2RT}{\pi M}} \tag{2}$$

where r is the pore radius, R is the gas constant, T is the temperature, and M is the molecular weight. According to these equations, molecular weight (M) of target gases and pore radius (r) of sensing film have a strong influence on the sensor response (S) to combustible gases. Increasing the pore radius (r) increases the sensor response, as easily expected from eqs 1 and 2. It is thus critical to control the pore radius when detecting large size gas molecules such as volatile organic compounds (VOCs). The VOC detection is important because of their detrimental effects on human health. Experimentally, large pores can be introduced in sensing films by tuning the size and morphology of constituting particles synthesized with various methods.[27,28] Calcination temperature control of sensing films also offers a way at changing the pore sizes.[29] Kida et al. synthesized monodispersed SnO_2 nanocrystals with different sizes using a seed-mediated growth technique to control the pore size of sensing films. They experimentally and theoretically revealed that increasing the pore size using larger crystals improved the sensor response to H_2S.[30]

However, increasing the film pore size using larger particles has an adverse effect. Larger particles usually have thin electron depletion layers on the surface, resulting in a lower change in electrical resistance upon reaction with gas molecules. In this study, to overcome this problem, we attempted to use nanoparticle clusters to produce gas sensing films with larger pores. The controlled clustering of nanoparticles is expected to create pores for efficient gas diffusion while retaining the crystallite size of nanoparticles, as shown in Scheme 1. We found that controlling the reaction solution pH produced clustered (aggregated) SnO_2 nanoparticles that were homogeneously dispersed in water. We also loaded Pd on clustered SnO_2 nanoparticles and examined their sensor responses to gases with different molecular sizes such as H_2, CO, and toluene (C_7H_8). The particular emphasis is to develop a new design of highly sensitive gas sensors on the basis of three key parameters such as particle size control, surface modification, and pore size control, as noted above.

EXPERIMENTAL SECTION

Synthesis of Monodispersed and Clustered SnO_2 Particles. Monodispersed SnO_2 nanoparticles were synthesized by a hydrothermal method.[31] Stannic acid gel ($SnO_2{\cdot}nH_2O$) was obtained by adding a $SnCl_4{\cdot}5H_2O$ solution (1 M) to a NH_4HCO_3 solution (1 M) in a dropwise manner according to the following reaction.

$$SnCl_4 + 4NH_4HCO_3 \rightarrow SnO_2{\cdot}nH_2O + 4NH_4Cl + (2 - n)H_2O \tag{3}$$

The obtained white gel precipitate was left overnight and then washed with a copious amount of distilled water to eliminate Cl^- included in the gel. The precipitate was dispersed in distilled water and then the solution pH was controlled with an NH_3 solution to 10.6. The concentration of stannic acid gel was constant at 2 wt % (200 mL). The reaction solution in a stainless steel vessel was hydrothermal treated at 200 °C for 3 h at 10 MPa, which was controlled by introducing nitrogen in the reactor. The solution was stirred at 600 rpm during hydrothermal treatment. These procedures produced a clear solution containing monodispersed SnO_2 nanoparticles. Clustered SnO_2 nanoparticles were prepared by decreasing the solution pH from 10.6 to 9.6 before hydrothermal treatment.

Synthesis of Pd-Loaded Monodispersed and Clustered SnO_2 Particles. $Pd[(NO_2)_2(NH_3)_2]$ was added into a solution containing stannic acid gel that was obtained by the above method and washed with deionized water. The solution pH was controlled to 9.3 to 10.6 with a NH_3 solution. The reaction solution in a Teflon-lined stainless steel vessel was hydrothermal treated at 200 °C for 3 h at 10 MPa.

Material Characterization. The obtained particles were analyzed by X-ray diffraction using Cu Kα radiation (XRD; RINT2100, Rigaku) and transmission electron microscopy (TEM; JEM-2000EX/T, JEOL). The crystallite sizes were estimated by Sherrer's equation using XRD

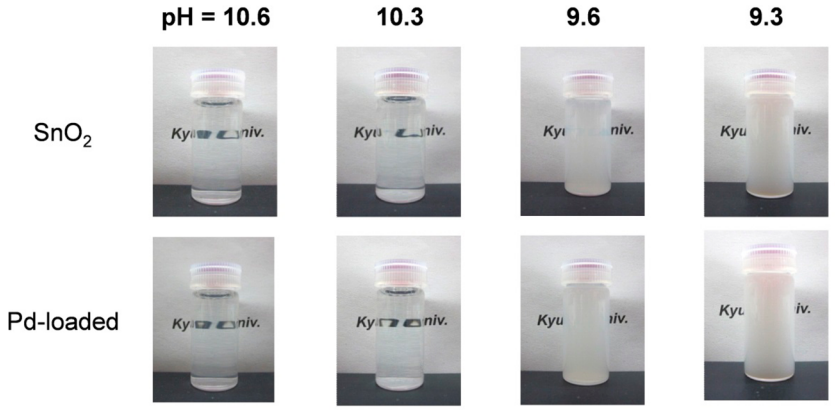

Figure 1. Photo images of suspensions containing Pd (0.1 mol %)-loaded or unloaded SnO_2 nanoparticles synthesized at different pH.

patterns. The size of the colloid particles was determined by dynamic light scattering (DLS) analysis using a DLS spectrophotometer (LPA-3000/3100, Otuka Electronics). The pore size distribution of the gas sensing films was obtained by the BJH (Barrett–Joyner–Halenda) method from adsorption/desorption isotherms. These were measured by the nitrogen gas adsorption method using a specific surface area/pore size distribution analyzer (BELSORP-mini II, Bel Japan). For this analysis, the films were fabricated on aluminum foil in the same manner as noted above and the foil was removed before the pore size distribution measurements. Inductively coupled plasma-atomic emission spectrometry (ICP-AES; SPS-1700HVR, Seiko Instruments Inc.) was used to determine the Pd loading amount on SnO_2 nanoparticles. For the ICP-AES analysis, samples were dissolved in aqua regia.

Preparation of Sensor Device and Evaluation of Sensor Response. Sensor devices were fabricated by a spin coating method where the obtained colloidal suspension was coated on alumina substrates (9 × 13 × 0.38 mm) equipped with a pair of comb-type Au microelectrodes (line width, 180 μm; distance between lines, 90 μm; sensing layer area, 64 mm^2). The thickness of the films was ca. 200 nm. The surfaces of the alumina substrates were treated with an ammonia solution containing H_2O_2 at 80 °C and then subjected to plasma cleaning (PS-601S, KASUGA ELECTRIC) before use. The Au electrodes were fabricated by screen-printing using a commercial Au paste followed by calcination at 850 °C prior to sensing film deposition. The sensing films were then deposited on the substrates and calcined at 600 °C for 3 h in air.

The sensing properties of the devices were examined using a conventional gas flow apparatus equipped with an electric furnace at a gas flow rate of 100 cm^3/min. The flow rates of air and sample gases were precisely controlled by mass flow controllers (SEC-series; HORIBA STEC). Sample gases of H_2, CO, and C_7H_8 in air were prepared by diluting parent synthetic gas mixtures with synthetic air. The parent synthetic gas mixtures were purchased from Sumitomo Seika Chemicals. Each sensor device was connected by a standard resistor in series and the voltage across the standard resistor was measured under an applied DC voltage of 4 V to evaluate the electrical resistance of the devices. An electrical signal was acquired from a sensor using an electrometer (2701; Keithley Instruments). The sensor response (S) was defined as the ratio of resistance in air (R_a) to that in air containing the combustible gases (R_g) ($S = R_a/R_g$).

RESULTS AND DISCUSSIONS

Characterization of Monodispersed and Clustered SnO_2 Particles. Transparent SnO_2 suspensions were obtained from $SnO_2 \cdot nH_2O$ by hydrothermal treatment at pH 10.6, as displayed in Figure 1 (top left). The dissolution of $SnO_2 \cdot nH_2O$ and crystallization of SnO_2 occurred under hydrothermal conditions at 200 °C to produce highly dispersed nanoparticles. In contrast, decreasing the solution pH from 10.6 to 9.3 decreased the transparency of the suspensions. At pH 9.3, the suspension was a turbid, milky white because of heavy light scattering of larger particles. These results indicate that particle aggregation occurred when solution pH was lowered. Indeed, ζ-potentials of the SnO_2 nanoparticles synthesized at pH 10.6 decreased when decreasing the solution pH, as shown in Figure 2. The decrease in the surface potential induced the

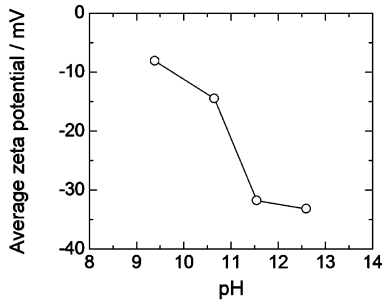

Figure 2. Dependence of ζ-potentials of SnO_2 nanoparticles in water on solution pH.

nanoparticle aggregation to form larger secondary particles. The above tendency was also observed for suspensions containing Pd (0.1 mol %)-loaded SnO_2 nanoparticles, as shown in Figure 1 (bottom), suggesting the homogeneous, highly dispersed deposition of Pd on SnO_2 with little influence on the particle aggregation behavior. Overall, the stability of all suspensions was good; no sedimentation of particles occurred. This property is very important to make homogeneous particulate films using the suspensions as a coating ink.

To verify the particle aggregation behavior, the colloidal sizes of SnO_2 nanoparticles loaded with and without Pd in the suspensions were measured by DLS, as shown in Figure 3. The average colloidal size of particles at pH 10.6 was determined to be 5.5 nm with a narrow size distribution, suggesting their good monodispersity. Here, we designate the particles synthesized at pH 10.6 as monodispersed nanoparticles. On the other hand, decreasing the solution pH from 10.6 to 9.3 increased the average colloidal size from 5.5 to 44 nm. The size distribution of aggregated particles is rather narrow, although heavily aggregated particles that are 200–500 nm can also be seen in the histogram. The presence of larger aggregated particles confirmed by DLS results is in good accordance with the visual appearance of the suspensions shown in Figure 1. Table 1 summarizes the colloidal size of SnO_2 nanoparticles synthesized

dx.doi.org/10.1021/am500944a | ACS Appl. Mater. Interfaces 2014, 6, 5319–5326

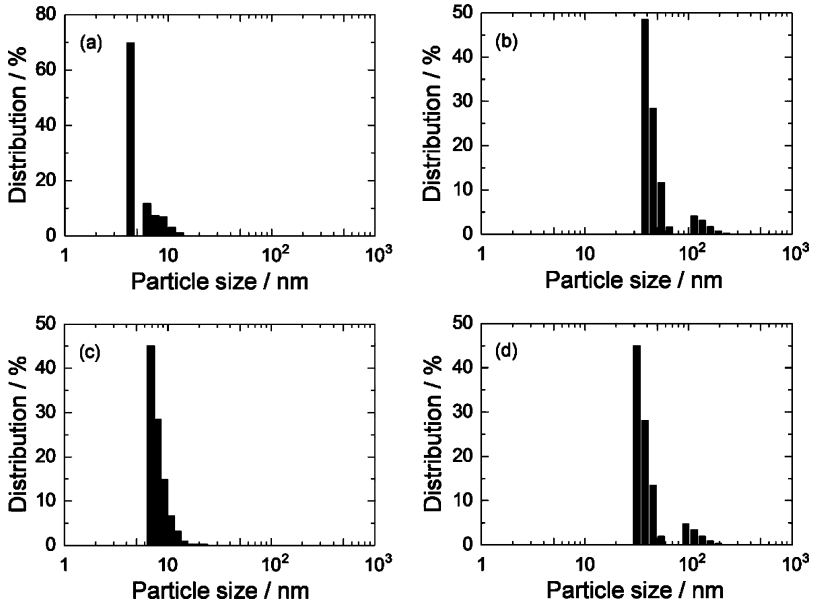

Figure 3. Particle size distribution of SnO_2 nanoparticles in suspensions prepared at (a) pH 10.6, (b) pH 9.3, (c) pH 10.6 with Pd, and (d) pH 9.3 with Pd.

Table 1. Crystallite and Colloidal Sizes of Pd-Loaded and Unloaded SnO_2 Nanoparticles Synthesized at Different pH[a]

sample	monodispersed SnO_2	clustered SnO_2	Pd-loaded monodispersed SnO_2	Pd-loaded clustered SnO_2	Pd-loaded clustered SnO_2
pH	10.6	9.6	10.6	9.3	9.3
Pd loading amount/mol %			0.1	0.1	0.2
crystallite size/nm	5	5	5	5	5
colloidal size/nm	5.5	44	8.2	46	46

[a]Crystallite and colloidal sizes were determined by Sherrer's equation using XRD peaks and by DLS measurements, respectively.

at different pH, together with those of Pd (0.1 and 0.2 mol %)-loaded SnO_2 nanoparticles. By introducing Pd, the colloidal size slightly increased from 5.5 to 8.2 nm. The average colloidal size is plotted as a function of solution pH for Pd-loaded and unloaded SnO_2 nanoparticles in Figure 4. The colloidal size

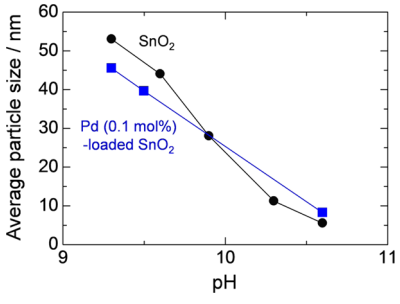

Figure 4. Average colloidal sizes for SnO_2 nanoparticles loaded with and without Pd as a function of solution pH used in the synthesis.

linearly increased as decreasing the solution pH for both cases. The DLS results confirmed that the aggregation behavior of Pd-loaded SnO_2 nanoparticles is almost the same as that for unloaded ones.

Figure 5 shows the XRD patterns of SnO_2 nanoparticles synthesized at pH 10.6 and 9.3 and Pd-loaded SnO_2 nanoparticles synthesized at pH 10.6 and 9.3. The XRD pattern matches that of tetragonal SnO_2 (JCPDS: 41-1445), and the broad peaks are indicative of the formation of nanosized SnO_2 crystals. The crystallite size of SnO_2 nano-

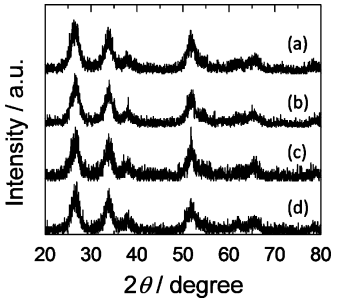

Figure 5. XRD patterns of SnO_2 nanoparticles synthesized at (a) pH 10.6, (b) pH 9.3, (c) pH 10.6 with Pd, and (d) pH 9.3 with Pd.

particles synthesized at pH 10.6 was 5.0 nm, obtained from XRD peaks using Scherrer's equation. This value is almost the same as that determined by DLS measurements (Figure 3a). Thus, the SnO_2 nanoparticles synthesized at pH 10.6 was single crystalline. Table 1 summarizes the crystallite size of SnO_2 nanoparticles synthesized at different pH, together with that of Pd (0.1 and 0.2 mol %)-loaded SnO_2 nanoparticles. It should be noted that the crystallite size did not change by decreasing the solution pH, despite the increase in the colloidal size. The Pd deposition also caused no change in the crystallite size.

The particle clustering (aggregation) by changing the solution pH was also investigated by TEM observation. Figure 6 shows TEM images of SnO_2 nanoparticles synthesized at pH 10.6 and 9.3. The particle size for pH 10.6 is estimated to be ca. 5 nm, in good agreement with the XRD results. In contrast, for pH 9.3, aggregated particles that are 30−60 nm in size can be

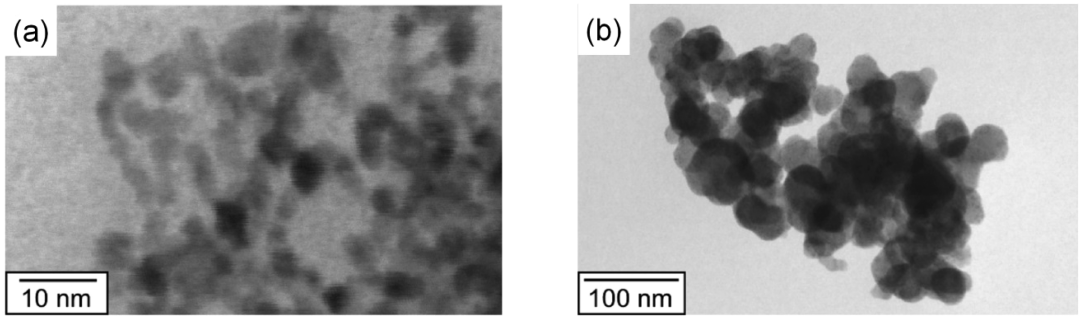

Figure 6. TEM images of SnO_2 nanoparticles synthesized at (a) pH 10.6 and (b) pH 9.3.

seen in the image. Each particle size is almost the same as that for particles synthesized at pH 10.6. From the DLS, XRD, and TEM results, we conclude that the nanoparticle aggregation occurred by decreasing the solution pH to produce larger secondary particles. Here, we designate the particles synthesized at pH 9.3 as clustered nanoparticles.

Gas Sensing Properties of Nanoporous Films Made Using Clustered SnO_2 Particles. We next studied the gas sensing behavior of films fabricated with the synthesized particles. Figure 7 shows the pore size distribution of films

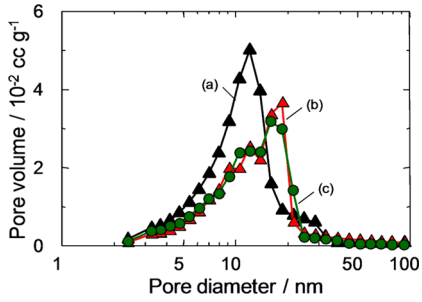

Figure 7. Pore size distribution of gas sensing SnO_2 films using (a) monodispersed nanoparticles, (b) clustered nanoparticles (c) Pd (0.1 mol %)-loaded clustered nanoparticles.

made from suspensions containing monodispersed, clustered, and Pd (0.1 mol %)-loaded clustered nanoparticles. Peak pore radii of films for monodispersed, clustered, and Pd-loaded clustered nanoparticles are 5.3, 9.3, and 8.0 nm respectively. By utilizing clustered nanoparticles for film fabrication, we successfully tuned the peak pore radius of the films due to the loose packing of the larger aggregated particles. On the other hand, no significant difference in peak pore radius occurred by Pd loading. This is because Pd loading did not affect the colloidal size of clustered nanoparticles, which is supported by the DLS results, as shown in Figure 4.

Figure 8 shows sensor responses (sensitivity) to 200 ppm H_2 and CO as a function of sensor operating temperature for four films made using monodispersed and clustered SnO_2 nanoparticles with and without Pd (0.1 mol %) loading. Average values obtained from two to three sensor responses from different devices are reported. The sensor responses went through a maximum at 300 °C for all devices. The volcano-shaped temperature dependence of the sensor response is typical for SnO_2-based gas sensors. This behavior has been theoretically explained by considering surface reactions and gas diffusion kinetics.[32] Increasing the operating temperature accelerates the surface reaction rate (k) of adsorbed oxygen with combustible gases, resulting in an increase in sensor

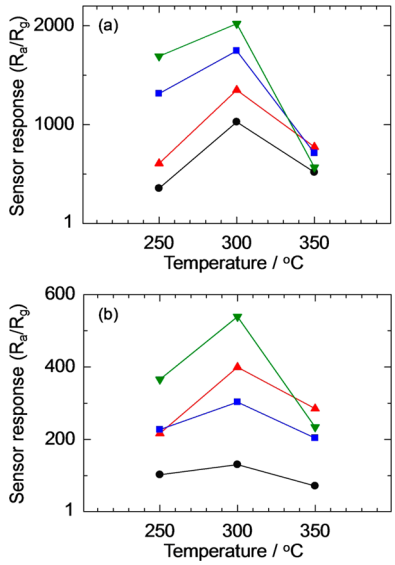

Figure 8. Sensor responses to (a) 200 ppm H_2 and (b) 200 ppm CO as a function of sensor operating temperature for SnO_2 films using (●) monodispersed nanoparticles, (▲) clustered nanoparticles, (■) Pd (0.1 mol %)-loaded monodispersed nanoparticles, and (▼) Pd (0.1 mol %)-loaded clustered nanoparticles.

response. However, further increasing the temperature impedes the diffusion of gases deep inside films because at higher temperatures gases tend to be consumed mainly at the surface of films due to the increased catalytic activity of SnO_2. The insufficient gas penetration within films lead to a decrease in the utility factor of the sensing films, decreasing the sensor response.

For H_2 detection, the monodispersed SnO_2 films showed the sensor response (S) of 1030, a 3 orders of magnitude change in the electrical resistance, at 300 °C, as shown in Figure 8a. By increasing the peak pore radius with clustered nanoparticles, the sensor response increased to S = 1350. Further sensitivity enhancement, reaching S = 1750 and 2020, was obtained by loading Pd onto monodispersed and clustered nanoparticles, respectively. For CO detection, almost the same trend was observed. The senor response to CO also increased using clustered nanoparticles formed by controlled particle aggregation, as shown in Figure 8b. Table 2 shows the calculated Knudsen diffusion coefficients (D_K) of H_2 and CO at 250, 300, and 350 °C in films having 5.3 and 9.3 nm pore radii, which correspond to those fabricated with monodispersed and clustered nanoparticles, respectively. It is confirmed that D_K for H_2 and CO significantly increases with increasing the pore radius from 5.3 to 9.3 nm. The calculation results also indicate

Table 2. Calculated Knudsen Diffusion Coefficients (D_K) of H_2, CO, and toluene (C_7H_8) at 350, 300, and 250°C in Sensing Films with Different Pore radii

		D_K(× 10^{12} nm^2·s^{-1})		
peak pore radius (nm)	temperature (°C)	H_2	CO	C_7H_8
5.28	350	9.02	2.42	1.33
	300	8.63	2.32	1.28
	250	8.25	2.21	1.22
9.3	350	15.9	4.25	2.35
	300	15.2	4.08	2.25
	250	14.5	3.9	2.15

that increasing the pore size is more influential at increasing D_K than increasing the operating temperature. As expected from eq 1, improving D_K results in large sensor responses, provided that k is constant. Therefore, we conclude that the enhanced sensor response is caused by an improvement in porosity of the films using clustered nanoparticles.

To know the effect of Pd loading on sensor response in more detail, we examined the dependence of sensor response on Pd loading amount. Figure 9 shows the sensor responses to 200 ppm H_2 and CO at 300 °C for films made with clustered nanoparticles. Maximum sensor responses were obtained at 0.1 mol % Pd loading. Yuasa et al. reported an optimum Pd loading amount of 0.1 mol % for Pd-loaded SnO_2 nanoparticles synthesized by a photochemical deposition method.[20] The reported results are in good agreement with the present case. The observed improvement in sensor response with such a low Pd loading amount suggests the highly homogeneous dispersion of Pd on clustered SnO_2 nanoparticles. However, further Pd loading resulted in a decrease in the sensor response. One probable reason is that H_2 and CO combusted mainly at the film surface due to the strong catalytic activity of Pd. This effect should be more pronounced at higher Pd loading amounts, hindering gas molecules from diffusing deep inside the sensing films. In contrast, at optimal Pd loading amounts at 0.1 mol %, gas molecules can efficiently penetrate within films, generating larger sensor responses by surface reaction, which is catalytically activated by Pd. The electrical sensitization of Pd should also contribute to the observed improvement in sensor response.

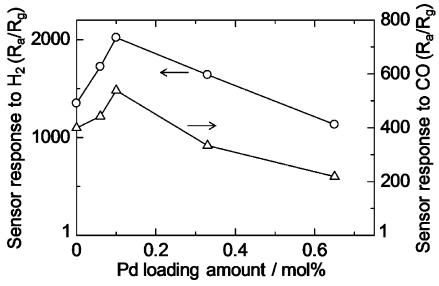

Figure 9. Sensor responses to 200 ppm H_2 and CO at 300 °C as a function of Pd loading amount for devices using clustered SnO_2 nanoparticles.

Figure 10 shows sensor responses to 50 ppm toluene as a function of sensor operating temperature for the films made using monodispersed and clustered SnO_2 nanoparticles with and without Pd loading. The clustered SnO_2 nanoparticles exhibited high sensor responses to toluene, reaching S = 1720 at 300 °C. As observed for CO and H_2 detection, the sensor

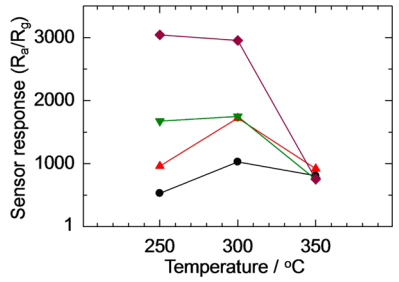

Figure 10. Sensor response to 50 ppm toluene as a function of operating temperature for SnO_2 films using (●) monodispersed nanoparticles, (▲) clustered nanoparticles, (▼) Pd (0.1 mol %)-loaded clustered nanoparticles, and (◆) Pd (0.2 mol %)-loaded clustered nanoparticles.

response was also improved by using the porous film made with clustered nanoparticles. This must be due to an improvement in D_K for toluene resulting from an increase in the film pore size, as calculated in Table 2. However, Pd loading at 0.1 mol % onto clustered nanoparticles was not sufficient at further improving the sensor response at 300 °C. It is known that toluene is more difficult to be combusted than CO and H_2.[33] Thus, loading Pd at higher amounts may be necessary to promote the reaction of toluene with adsorbed oxygen. It is considered that the lower reactivity of toluene possibly allows for its diffusion deep inside the sensing films without experiencing combustion reaction. In this regard, increasing the pore size should exert a considerable impact on the toluene diffusion. The obtained results confirm that improving the gas diffusivity in sensing films by the pore size control is effective at detecting large size gas molecules such as toluene. However, at 350 °C, almost no difference in sensor response was observed for all films. It is likely that toluene predominantly combusted at the surface of the films at higher temperatures, significantly decreasing the utility factor of the films.

To check the ability of the developed sensor to detect toluene at low concentrations, we examined the dependence of the sensor response on toluene concentration. Figure 11 shows the calibration curve of the sensor response at 300 °C in a log–log scale for Pd (0.2 mol %)-loaded clustered SnO_2 nanoparticles. A straight calibration curve was obtained by plotting measured sensor responses against toluene concentration (64 to 50 000 ppb). The detection limit of toluene can roughly be determined to be 2.5 ppb by extrapolating the sensor responses to the value of 1.0 (baseline in air). The estimated detection limit is very low, indicating the high

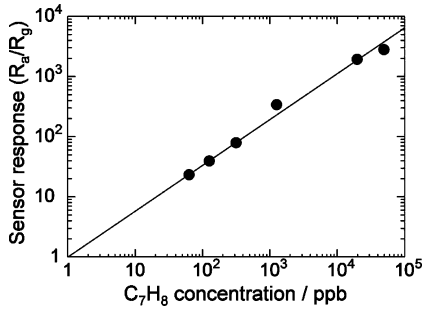

Figure 11. Sensor calibration curve for the device using Pd (0.2 mol %)-loaded clustered SnO_2 nanoparticles. The curve was obtained from sensor responses as a function of toluene concentration at 300 °C.

dx.doi.org/10.1021/am500944a | ACS Appl. Mater. Interfaces 2014, 6, 5319–5326

sensitivity of our sensor. In Japan, the guideline value for indoor air concentration of toluene is 70 ppb, which was set up based on its chronic toxicity by the Ministry of Health, Labor and Welfare. Thus, the results indicate the promising capability of our sensor for monitoring toluene concentrations in home and work places to avoid indoor air pollution by VOCs. Further studies on the selectivity and stability assessment are necessary to develop practically feasible VOC sensors.

CONCLUSION

Clustered SnO_2 nanoparticles were successfully synthesized from $SnO_2 \cdot nH_2O$ as a precursor by a hydrothermal method, where preformed nanocrystals (ca. 5 nm) were aggregated to produce larger secondary particles (ca. 45 nm) under hydrothermal conditions at pH 9.3. Adding Pd-$[(NH_3)_2(NO_2)_2]$ to the precursor solution readily produced Pd-loaded SnO_2 nanoparticle clusters. Thin film sensor devices were fabricated by a spin-coating method using the clustered SnO_2 nanoparticles loaded with Pd. The sensor devices using clustered nanoparticles showed improved sensor responses to H_2 and CO compared with those using monodispersed nanoparticles. This is due to an enhancement in the porosity of the sensing film, as evidenced by pore size distribution measurements that showed the peak pore size of the film increased by using larger clustered nanoparticles. Pd loading further increased the sensor response due to the catalytic and electrical sensitization effects of Pd. More importantly, the Pd-loaded SnO_2 nanoparticle clusters showed significantly high sensitivity to toluene due to the enhanced diffusivity in the sensing film, reaching a very low detection limit of 2.5 ppb.

AUTHOR INFORMATION

Corresponding Author

*K. Suematsu. E-mail: suematsu.koichi.682@m.kyushu-u.ac.jp.

Notes

The authors declare no competing financial interest.

ACKNOWLEDGMENTS

This work was supported a Grant-in-Aid for Scientific Research (B) (No. 22350064) from the Ministry of Education, Culture, Sports, Science and Technology of Japan. T.K. also thanks the financial support from Foundation for Promotion of Material Science and Technology of Japan (MST).

REFERENCES

(1) Kida, T.; Doi, T.; Shimanoe, K. Synthesis of Monodispersed SnO_2 Nanocrystals and Their Remarkably High Sensitivity to Volatile Organic Compounds. *Chem. Mater.* **2010**, *22*, 2662−2667.

(2) Tanaka, K.; Morimoto, T.; Sonoda, S.; Matsuura, S.; Moriya, K.; Egashira, M. Combustion Monitoring Sensor Using Tin Dioxide Semiconductor. *Sens. Actuators, B* **1991**, *3*, 247−253.

(3) Kolmakov, A.; Klenov, D. O.; Liach, Y.; Stemmer, S.; Moskovits, M. Enhanced Gas Sensing by Individual SnO_2 Nanowires and Nanobelts Functionalized with Pd Catalyst Particles. *Nano Lett.* **2005**, *5* (4), 667−673.

(4) Chiu, H. C.; Yeh, C. S. Hydrothermal Synthesis of SnO_2 Nanoparticles and Their Gas-sensing of Alcohol. *J. Phys. Chem. C* **2007**, *111*, 7256−7259.

(5) Kamiuchi, N.; Matsui, T.; Yamaguchi, N.; Muroyama, H.; Matsui, T.; Kikuchi, R.; Eguchi, K. Activation of Pt/SnO_2 Catalyst for Catalytic Oxidation of Volatile Organic Compounds. *Catal. Today* **2010**, *157*, 415−419.

(6) Iglesias-Juez, A.; Kubacka, A.; Fernandez-Garcia, M.; Di Michiel, M.; Newton, M. A. Nanoparticulate Pd Supported Catalysts: Size-Dependent Formation of Pd(I)/Pd(0) and Their Role in CO Elimination. *J. Am. Chem. Soc.* **2011**, *133*, 4484−4489.

(7) Kar, A.; Kundu, S.; Patra, A. Surface Defect-Related Luminescence Properties of SnO_2 Nanorods and Nanoparticles. *J. Phys. Chem. C* **2011**, *115*, 118−124.

(8) Dou, X.; Sabba, D.; Mathew, N.; Wong, L. H.; Lam, Y. M.; Mhaisalkar, S. Hydrothermal Synthesis of High Electron Mobility Zn-doped SnO_2 Nanoflowers as Photoanode Material for Efficient Dye-Sensitized Solar Cells. *Chem. Mater.* **2011**, *23*, 3938−3945.

(9) Wang, W. W.; Zhu, Y. Y.; Yang, L. X. ZnO-SnO_2 Hollow Spheres and Hierarchical Nanosheets: Hydrothermal Preparation, Formation Mechanism, and Photocatalytic Properties. *Adv. Funct. Mater.* **2007**, *17*, 59−64.

(10) Olivi, P.; Pereira, E. C.; Longo, E.; Varella, J. A.; Bulhoes, L. O. S. Preparation and Characterization of a Dip-Coated SnO_2 Film for Transparent Electrodes for Transmissive Electrochromic Devices. *J. Electrochem. Soc.* **1993**, *140*, 81−82.

(11) Shim, T. S.; Moon, H. G.; Kim, D. H.; Jang, H. W.; Kang, C. Y.; Yoon, Y. S.; Yoon, S. J. Transparent Conducting Oxide Electrodes for Novel Metal Oxide Gas Sensors. *Sens. Actuators, B* **2011**, *160*, 357−363.

(12) Zhu, J.; Lu, Z.; Aruna, S. T.; Aurbach, D.; Gedanken, A. Sonochemical Synthesis of SnO_2 Nanoparticles and Their Preliminary Study as Li Insertion Electrodes. *Chem. Mater.* **2000**, *12*, 2557−2566.

(13) Wang, J.; Du, N.; Zhang, H.; Yu, J.; Yang, D. Large-Scale Synthesis of SnO_2 Nanotube Arrays as High-Performance Anode Materials of Li-Ion Batteries. *J. Phys. Chem. C* **2011**, *115*, 11302−11305.

(14) Chen, J.; Yano, K. Highly Monodispersed Tin Oxide/Mesoporous Starbust Carbon Composite as High-Performance Li-Ion Battery Anode. *ACS Appl. Mater. Interfaces* **2013**, *5*, 7682−7687.

(15) Fujihara, S.; Maeda, T.; Ohgi, H.; Hosono, E.; Imai, H.; Kim, S. Hydrothermal Routes To Prepare Nanocrystalline Mesoporous SnO_2 Having High Thermal Stability. *Langmuir* **2004**, *20*, 6476−6481.

(16) Taguchi, N. Japanese Patent No. 47-38840, 1963.

(17) Xu, C.; Tamaki, J.; Miura, N.; Yamazoe, N. Grain Size Effects on Gas Sensitivity of Porous SnO_2-Based Elements. *Sens. Actuators, B* **1991**, *3*, 147−155.

(18) Yamazoe, N.; Shimanoe, K. Roles of Shape and Size of Component Crystals in Semiconductor Gas Sensors I. Response to Oxygen. *J. Electrochem. Soc.* **2008**, *155*, J85−J92.

(19) Yamazoe, N.; Shimanoe, K. Roles of Shape and Size of Component Crystals in Semiconductor Gas Sensors II. Response to NO_2 and H_2. *J. Electrochem. Soc.* **2008**, *155*, J93−J98.

(20) Yuasa, M.; Kida, T.; Kengo, S. Preparation of a Stable Sol Suspension of Pd-Loaded SnO_2 Nanocrystals by a Photochemical Deposition Method for Highly Sensitive Semiconductor Gas sensors. *ACS Appl. Mater. Interfaces* **2012**, *4*, 4231−4236.

(21) Krivetskiy, V.; Ponzoni, A.; Comini, E.; Badalyan, S.; Rumyantseva, M.; Gaskov, A. Selectivity Modification of SnO_2-Based Materials for Gas Sensor. *Electroanalysis* **2010**, *22*, 2809−2816.

(22) Sahm, T.; Rong, W.; Bârsan, N.; Mädler, L.; Weimar, U. Sensing of CH_4, CO and Ethanol with in Situ Nanoparticle Aerosol-Fabricated Multilayer Sensors. *Sens. Actuators, B* **2007**, *127*, 63−68.

(23) Koziej, D.; Hübner, M.; Barsan, N.; Weimar, U.; Sikora, M.; Grunwaldt, J. D. Operando X-ray Adsorption Spectroscopy Studies on Pd-SnO_2 Based Sensors. *Phys. Chem. Chem. Phys.* **2009**, *11*, 8620−8625.

(24) Safonova, O. V.; Neisius, T.; Ryzhikov, A.; Chenevier, B.; Gaskov, A. M.; Labeau, M. Characterization of the H_2 Sensing Mechanism of Pd-Promoted SnO_2 by XAS in Operando Conditions. *Chem. Commun.* **2005**, *2005*, 5202−5204.

(25) Hübner, M.; Koziej, D.; Grunwaldt, J. D.; Weimar, U.; Barsan, N. An Au Clusters Related Spill-Over Sensitization Mechanism in SnO_2-Based Gas Sensors Identified by Operando HERFD-XAS, Work Function Changes, DC Resistance and Catalytic Conversion Studies. *Phys. Chem. Chem. Phys.* **2012**, *14*, 13249−13254.

(26) Sakai, G.; Matsunaga, N.; Shimanoe, K.; Yamazoe, N. Theory of Gas-Diffusion Controlled Sensitivity for Thin Film Semiconductor Gas Sensor. *Sens. Actuators, B* **2001**, *80*, 125−131.
(27) Wang, H.; Liang, Q.; Wang, W.; An, Y.; Li, J.; Guo, L. Preparation of Flower-Like SnO_2 Nanostructures and Their Applications in Gas-Sensing and Lithium Storage. *Cryst. Growth. Des.* **2011**, *11*, 2942−2947.
(28) Wang, H.; Liang, J.; Fan, H.; Xi, B.; Zhang, M.; Xiong, S.; Zhu, Y.; Qian, Y. Synthesis and Gas Sensitivities of SnO_2 Nanorods and Hollow Microspheres. *J. Solid State Chem.* **2008**, *181*, 122−129.
(29) Jin, Z.; Zhou, H. J.; Jin, Z. L.; Savinell, R. F.; Liu, C. C. Application of Nano-Crystalline Porous Tin Oxide Thin Film for CO Sensing. *Sens. Actuators, B* **1998**, *52*, 188−194.
(30) Kida, T.; Fujiyama, S.; Suematsu, K.; Yuasa, M.; Shimanoe, K. Pore and Particle Size Control of Gas Sensing Synthesized by Seed-Mediated Growth: Design of Highly Sensitive Gas Sensors. *J. Phys. Chem. C* **2013**, *117*, 17574−17582.
(31) Baik, N. S.; Sakai, G.; Shimanoe, K.; Miura, N.; Yamazoe, N. Hydrothermal Treatment of Tin Oxide Sol Solution for Preparation of Thin-Film Sensor with Enhanced Thermal Stability and Gas Sensitivity. *Sens. Actuators, B* **2000**, *65*, 97−100.
(32) Yamazoe, N.; Sakai, G.; Shimanoe, K. Oxide Semiconductor Gas Sensors. *Catal. Surv. Asia* **2003**, *7*, 63−75.
(33) Aguero, F. N.; Barbero, B. P.; Gambaro, L.; Cadus, L. E. Catalytic Combustion of Volatile Organic Compounds in Binary Mixtures over $MnOx/Al_2O_3$ Catalyst. *Appl. Catal., B* **2009**, *91*, 108−112.